

2016

DLVO Approximation Methods for Predicting the Attachment of Silver Nanoparticles to Ceramic Membranes

Anne M. Mikelonis

Sungmin Youn
Marshall University, youns@marshall.edu

Desmond F. Lawler

Follow this and additional works at: http://mds.marshall.edu/wde_faculty

 Part of the [Nanoscience and Nanotechnology Commons](#), and the [Other Engineering Commons](#)

Recommended Citation

Mikelonis, A. M., Youn, S., & Lawler D. F. (2016). DLVO approximation methods for predicting the attachment of silver nanoparticles to ceramic membranes. *Langmuir*, 32 (7), 1723–1731. doi:10.1021/acs.langmuir.5b04675

This Article is brought to you for free and open access by the Weisberg Division of Engineering at Marshall Digital Scholar. It has been accepted for inclusion in Weisberg Division of Engineering Faculty Research by an authorized administrator of Marshall Digital Scholar. For more information, please contact zhangj@marshall.edu, martj@marshall.edu.

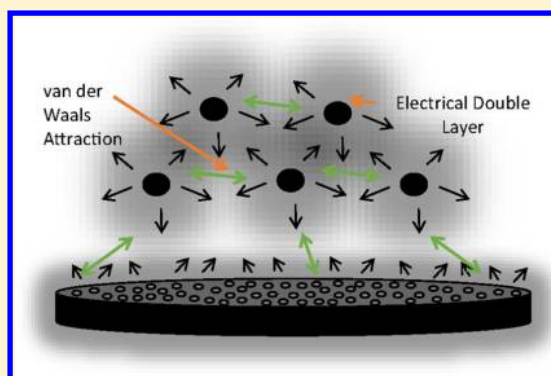
DLVO Approximation Methods for Predicting the Attachment of Silver Nanoparticles to Ceramic Membranes

Anne M. Mikelonis,* Sungmin Youn, and Desmond F. Lawler

Department of Civil, Architectural, and Environmental Engineering, The University of Texas at Austin, 301 E. Dean Keeton Street, Mail Stop C1786, Austin, Texas 78712-1173, United States

Supporting Information

ABSTRACT: This article examines the influence of three common stabilizing agents (citrate, poly(vinylpyrrolidone) (PVP), and branched poly(ethylenimine) (BPEI)) on the attachment affinity of silver nanoparticles to ceramic water filters. Citrate-stabilized silver nanoparticles were found to have the highest attachment affinity (under conditions in which the surface potential was of opposite sign to the filter). This work demonstrates that the interaction between the electrical double layers plays a critical role in the attachment of nanoparticles to flat surfaces and, in particular, that predictions of double-layer interactions are sensitive to boundary condition assumptions (constant charge vs constant potential). The experimental deposition results can be explained when using different boundary condition assumptions for different stabilizing molecules but not when the same assumption was assumed for all three types of particles. The integration of steric interactions can also explain the experimental deposition results. Particle size was demonstrated to have an effect on the predicted deposition for BPEI-stabilized particles but not for PVP.



INTRODUCTION

A recent trend in membrane research is the attachment of nanoparticles (NPs) to the membrane's surface to harness the NPs' reactive and catalytic properties.^{1–3} NPs such as silver (Ag), iron, titanium, and magnesium oxides are often studied because they impart useful features such as the degradation/removal of challenging contaminants (e.g., arsenic, trichloroethylene, nitrobenzene, and lead) or a reduction in total organic carbon, a precursor for disinfection byproducts formed after chlorination in drinking water treatment.^{4–6} In particular, Ag NPs, the focus of this study, have garnered substantial attention in terms of disinfection and biofouling reduction on ceramic water filters.^{7–9} Although it is well known that particle deposition onto surfaces is a complex process that involves many factors such as particle size, surface charge heterogeneity, surface roughness, and steric and hydrophobic interactions, electrostatic interactions are expected to play a significant role in the process.^{10,11} The objective of this work is to evaluate if approximations of Derjaguin–Landau–Verwey–Overbeek (DLVO) theory can accurately predict the relative tendency of Ag NP deposition onto ceramic membranes for particles stabilized by different organic ligands. A combination of experimental and modeling approaches were used to test two hypotheses: (1) pH conditions can be selected which promote attachment (for one particular type of NP to ceramic membranes) and (2) Ag NP/ceramic membrane systems with lower predicted DLVO energy barriers will experience

greater Ag deposition (where each system is a different type of Ag NP).

Background. NPs are generated by a wide range of techniques, many of which use stabilizing molecules during synthesis to prevent aggregation and provide surface passivation. Stabilization of the metal core is provided through one of three primary mechanisms: electrostatic, steric, or electrosteric interactions between the metal and stabilizer.¹² In an extensive review of the literature,¹³ the most common agents used by researchers to stabilize Ag NPs were citrate at 27% use, followed by poly(vinylpyrrolidone) (PVP) at 18% and amines at 8%. These coatings produce diverse conformations and charge distributions on the particle surface, which in turn affect particle–particle and particle–flat surface interactions. Currently, stabilizers are selected using arduous trial-and-error methods with the majority of synthesis goals focused on size and shape control rather than postprocessing attachment to surfaces. Although a few studies have demonstrated differences in toxicity due to the NP's stabilizing agent,^{14,15} the influence of stabilizer structure is normally neglected in the literature because stabilizer properties are challenging to measure with routine analytical methods. The small size and large curvature of NPs present measurement challenges and require several advanced complementary analysis methods such as atomic

Received: December 21, 2015

Revised: January 18, 2016

Published: January 21, 2016

force microscopy (AFM), X-ray photoelectron spectroscopy (XPS), transmission electron microscopy (TEM), scanning transmission electron microscopy (STEM), and thermal gravimetric analysis (TGA) to glean useful information about the thickness and density distribution of the stabilizer. Consequently, the incorporation of steric forces into deposition models is limited due to practical constraints, whereas the more straightforward measurements of surface potential and size required for DLVO calculations are more accessible. As a result, the identification of situations where DLVO theory is useful in controlling NP deposition holds great potential for routine application in a wide range of disciplines.

DLVO Exact Solution. DLVO theory predicts colloidal stability by summing the potential energy associated with the interaction of the electrical double layers of two surfaces and the van der Waals interactions.¹⁶ The calculation of the van der Waals energies for a particle (p) and flat surface (f) is relatively straightforward

$$V_{A,pf} = \frac{Aa_p}{6s} \left(1 + \frac{14s}{\lambda} \right)^{-1} \quad (1)$$

where s represents the separation distance, A is the Hamaker constant, λ is the characteristic wavelength of interaction, and a_p is the particle radius.¹⁰ A value of 100 nm is typically appropriate for λ .¹⁷ The value of the Hamaker constant is uncertain in the van der Waals energy calculation because the role of the particle core versus the outer stabilizing layer is not clearly understood. The applicability of only the core material value of the Hamaker constant is dependent on the stabilization mechanism. For particles stabilized electrostatically by small molecules (e.g., citrate), the Hamaker constant is not drastically different from the value for the core material alone.^{18,19} On the other hand, it is recognized that steric and electrosterically stabilized particles would require a different effective Hamaker constant. Nevertheless, since no better method has been developed, it is still common practice to use only the core metal for the calculation, regardless of the nature of the stabilizer.^{20,21}

The exact computation of the energy associated with the double layers is much more complicated and requires numerical methods. Furthermore, to solve for the energy associated with the overlapping double layers, it is necessary to specify if the charged surfaces are at constant surface potential or at constant surface charge upon approach. The use of one assumption over the other reflects different views of the relevant physical phenomena at close separation distances. For example, counterions can adsorb as the two surfaces grow nearer or escape because of the geometry of the surfaces (with the constant potential assumption being more applicable), particles such as clays and latex can have a fixed charge (with the constant charge assumption being more applicable), or interactions of double layers may be so brief under Brownian motion that equilibrium is maintained (with the constant charge assumption being more applicable).²² At large separation distances, regardless of which assumption is made, the calculated interaction energies for the exact solution are in close agreement. However, the two assumptions lead to drastic differences in energies of interaction at short separation distances, differences which are magnified when the potentials are of different magnitudes for each surface. Intuitively perplexing is that unequal surface potentials with the same sign will provide attraction at small separation distances under the constant potential assumption, and repulsion will occur for

opposite sign surface potentials with the constant charge assumption.²³ In general, the constant surface charge assumption can be considered to be an upper limit to the possible energy of interaction, whereas the constant surface potential corresponds to the lower limit.¹⁶

DLVO Double-Layer Approximations. For routine use, such as selecting the optimal NP attachment conditions, it is more convenient to use an approximate expression than numerical methods required for the exact solution.²⁴ Approximation methods still face the issue of disagreement at short separation distances between the constant potential and constant charge assumption. The linear superposition approximation (LSA), an approximation method that can use either the constant charge or constant potential assumptions, always lies somewhere in the middle (Figure 1). An alternative model,

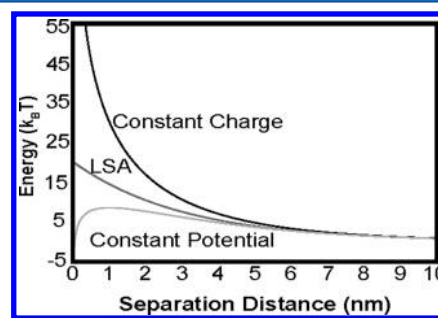


Figure 1. Electrical double layer energy of interaction for a particle (33.8 mV) and a flat plate (14.5 mV) under the BPEI Ag NP experimental condition. The graph demonstrates the solution dependence on the boundary condition assumption employed during the calculation. The top line shows the constant charge assumption, and the bottom line, the constant potential assumption. The line in the middle is a linear superposition approximation, an improvement to the constant potential approximation.

charge regulation, is based upon capacitance and accounts for the loss of species through adsorption. It requires knowledge of a regulation parameter for a particular surface type.^{25,26} Care must be taken to use the scenarios within the bounds of acceptable error for each particular application because the approximations, particularly linearized versions, add more limitations to the magnitude and sign of the charges/surface potentials. Additionally, the double-layer interaction energy is geometry specific and, for the scenario at hand, must be adapted to a particle and a flat plate configuration. An extensive body of work in the field of environmental engineering examines particle removal in aqueous solutions using granular media filtration. At the microscopic level, the size difference between the particles and the grains of the filter medium are so great that the particle “sees” the filter medium as a flat plate, just as the NPs interact with the surface of a membrane in this study. The equations for the most frequently used approximation methods are summarized in Table 1 and discussed subsequently. Additionally, a very detailed discussion of particle–particle electrical-double layer approximations can be found in Elimelech et al.²⁷

For the constant charge assumption, two approximation methods have been developed. The compression method (eq 2a) uses the notion that as the two surfaces approach each other the charge density in the region between the surfaces increases. Using the Poisson equation, which relates charge to potential, estimates of the potential as it changes at different

Table 1. Electrical Double Layer Approximation Methods^a

assumption	method	geometry	double layer interaction energy (V)	references
constant charge	compression method	flat plate–flat plate	$V_{R,ff} = \frac{2nk_B T}{\kappa} \left[(y_1 + y_2) \ln \left(\frac{B + \left(\frac{y_1 + y_2}{2}\right) \coth\left(\frac{\kappa s}{2}\right)}{1 + \left(\frac{y_1 + y_2}{2}\right)} \right) - \ln \left(\left(\frac{y_1 + y_2}{2}\right)^2 + \cosh \kappa s + B \sinh \kappa s \right) + \kappa s \right]$ $B = \sqrt{\left[1 + \left(\frac{y_1 + y_2}{2}\right)^2 \operatorname{csch}^2\left(\frac{\kappa s}{2}\right) \right]}$	(2a) 23
	linearized Poisson–Boltzmann	particle–particle	$V_{R,pp} = \frac{a_{p1} a_{p2}}{a_{p1} + a_{p2}} \frac{2\pi n k_B T}{\kappa^2} (y_1^2 + y_2^2) \left[\frac{2y_1 y_2}{y_1^2 + y_2^2} \ln \left(\frac{1 + e^{-\kappa s}}{1 - e^{-\kappa s}} \right) - \ln[1 - e^{-2\kappa s}] \right]$	(3) 28
	linearized Poisson–Boltzmann	particle–flat plate	$V_{R,pf} = \pi \epsilon_0 \epsilon_r a_p \left\{ \begin{aligned} & 2\Psi_{df} \Psi_{dp} \ln \left[\frac{1 + e^{(-\kappa s)}}{1 - e^{(-\kappa s)}} \right] - \\ & (\Psi_{df}^2 + \Psi_{dp}^2) \ln[1 - e^{(-2\kappa s)}] \end{aligned} \right\}$	(4) ^b
constant potential	linearized Poisson–Boltzmann	particle–flat plate	$V_{R,pf} = \pi \epsilon_0 \epsilon_r a_p \left\{ \begin{aligned} & 2\Psi_{df} \Psi_{dp} \ln \left[\frac{1 + e^{(-\kappa s)}}{1 - e^{(-\kappa s)}} \right] + \\ & (\Psi_{df}^2 + \Psi_{dp}^2) \ln[1 - e^{(-2\kappa s)}] \end{aligned} \right\}$	(5) 29
	linear superposition approximation (LSA)	particle–flat plate	$V_{R,pf} = a_{p1} \frac{128\pi n k_B}{\kappa^2} \gamma_1 \gamma_2 e^{-\kappa s}$	(6a) ^c
			$\gamma = \tanh(y/4)$	(6b)

^a ϵ represents permittivity, a_p the represents the particle radius, s represents the separation distance, Ψ represents the surface potential, κ represents the Debye length, n represents the number concentration, $\kappa^2 = 2e^2 n z^2 / \epsilon k_B T$, and $y = ze\Psi/k_B T$ (e is the elementary charge and z is the valency of the ions in solution). The y value corresponds to the reduced dimensionless form of the surface potential Ψ . ^bGeometry converted from ref 28 and notation transformed to be in terms of potential. ^cGeometry converted from ref 23.

separation distances can be made without direct measurement. The compression method has been shown to agree very well with exact solutions for plates of both equal and unequal double layers.^{22,23} Unfortunately, the expression developed using the compression method cannot be easily integrated (which is necessary to change geometry). If numerical methods are to be avoided, then it is helpful only in solving for double layer interaction energies of two flat plates. A linearized version of the Poisson–Boltzmann equation has also been developed for the constant charge assumption and is employed in this paper (eq 4).²⁸ It overestimates the repulsion at close approach because the linearization is based on a simplification of the Taylor series where only the two first terms are considered. This assumption leads to error if the surface potential is greater than 125 mV.³⁰ At short separation distances, the linearization at constant charge can be problematic for certain scenarios. For two oppositely charged surfaces, the energy of interaction will become repulsive at constant potential. However, the constant charge linearization captures attraction between oppositely charged surfaces at these short separation distances where other approximations can be problematic for certain scenarios.

For the constant potential assumption, a linearized version of the Poisson–Boltzmann equation and the Derjaguin approximation is also used to solve for the energy of interaction (eq 5). For water treatment applications, most researchers use the work derived by Hogg et al.²⁹ These calculations require

relatively straightforward measurements of particle size and the surface potential for the particle and the flat plate collector. As previously mentioned for the linearization at constant charge, the assumptions made during the derivation require that the surface potentials be less than 125 mV and similar in value to give good agreement with the exact solution for short separation distances (which is where the energy barrier occurs). While this method has proven applicable in many environmental engineering situations, where natural organic matter is ubiquitous and coats both surfaces, rendering them similar, the relationship is limited for the more pristine manufacturing conditions where NPs, due to stabilizing agents, have very different surfaces than the membrane. NPs by design often have large surface potentials in order to prevent aggregation and also have a different surface charge than the membrane.

LSA (eq 6a) can use either the assumption of constant potential or constant charge but is most frequently used with constant potential to correct for the underestimation of the energy barrier at short separation distances. LSA, with the constant potential assumption, has been found to be applicable for situations of particle deposition.¹¹ It assumes that each surface is isolated but that a region exists between the two surfaces where potential is small and obeys the linearized Poisson–Boltzmann equation. This allows contributions from each surface to be added to obtain an overall potential energy.²⁷ The advantages of the LSA model are that it is valid for any

arbitrary surface potentials, electrolyte composition, and particle size and does not underestimate the energy barrier like the linearized Poisson–Boltzmann estimation method for constant potential does.¹¹ It adheres to derivation assumptions for small surface potentials and separation distances of $ks > 1$.²³

A few items are important to note about the approximations. First, by convention, negative energies represent attraction and positive energies represent repulsion. Second, after converting to a particle and flat plate, it is possible to cast eq 3 in terms of surface potential (the experimentally estimated variable). One will observe that the only difference between eqs 4 and 5 is that, at constant surface potential, the $(\Psi_{d_r}^2 + \Psi_{d_p}^2) \ln[1 - e^{(-2ks)}]$ term is added, whereas it is subtracted at constant charge. This difference explains why the constant surface potential underestimates its' exact solution for unequal and high surface potentials, but the constant charge leads to overestimates of its' exact solution of repulsion at close approach for surfaces that are of unequal and/or high surface potential (in good agreement with exact solutions for attractive scenarios).

In summary, the most widely used and accessible approximations are based on the linearized Poisson–Boltzmann equation. At constant charge, the energy barrier is overestimated, whereas at constant potential, the energy barrier is underestimated at short separation distances. The underestimation at constant potential can be corrected in part by using the LSA method. In reality, it is challenging to know which extreme case, constant charge or constant potential, or some intermediate scenario is likely to occur, so all scenarios should be considered.

EXPERIMENTAL SECTION

Materials. Trace-metal-grade HNO_3 , standardized KOH, NIST-traceable Ag ICP standard, and ACS-grade reagents were used for the experiments reported. Citrate, 40 K PVP, and 1800 Da molecular weight branched poly(ethylenimine) (BPEI)-stabilized Ag NPs were synthesized in our laboratory and used for this study. These stabilizing agents were selected to represent the three common modes of stabilization: electrostatic (citrate), steric (PVP), and electrosteric (BPEI). Synthesis methods, cleaning procedures, images, and zeta potential values for the particles at different pH values are available in the [Supporting Information](#). BPEI-stabilized Ag NPs were found to have an average stabilizer coating thickness of 10 nm; PVP Ag NPs, 3 nm; and citrate Ag NPs, 2 nm. STEM images, with stabilizer thickness noted, are also provided in the [Supporting Information](#). A more precise quantification of stabilizer thickness is possible with more advanced techniques, but this method was considered to be reasonable for the purposes of this research. Representative particle size distributions obtained using multiple images taken on a FEI Tecnai TEM with ImageJ software indicate that, on average, the particles are 10–15 nm in diameter (Figure 2a). The particles aggregate at different rates under the experimental conditions used in this study (Figure 2b,c). The aggregation rates are used later in the article to estimate particle sizes at experimentally relevant time points.

Porous aluminum oxide (Al_2O_3) ceramic disks with an effective pore size of 0.1 μm (diameter) and a disk diameter of 13 mm (Whatman Anodiscs) were used as substrates in this work. The Al_2O_3 Anodiscs have highly uniform porosity created via an anodic oxidation of aluminum metal foil in a process similar to that described by Furneaux et al.³¹ The point of zero charge (pzc) for the Anodisc is at a pH of approximately 5.5 (Figure 3). Those familiar with colloidal α -alumina particles (pzc 7–9) might notice that the Anodisc has a significantly lower pzc; the disparity arises from differences in the surface coordination of hydroxyl groups for particles versus planar surfaces.³² It is therefore important to avoid using particles for experiments representing porous, flat surfaces.

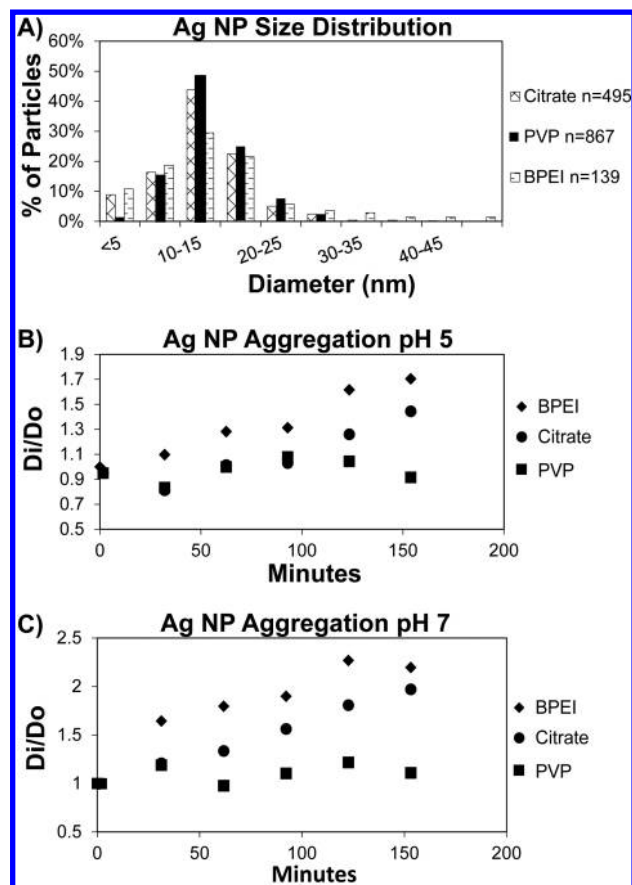


Figure 2. (A) Ag NP size analysis from multiple images analyzed using ImageJ. (B, C) Ag NP aggregation rates determined using a NanoSight particle size analyzer at a constant ionic strength of 10 mM, added as KNO_3 . (B) At pH 5 and (C) at pH 7.

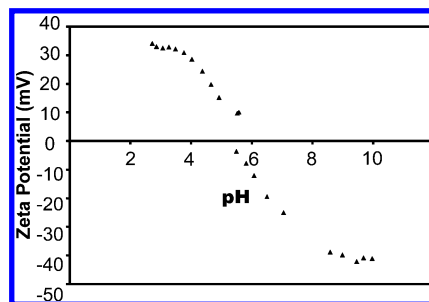


Figure 3. Zeta potential of a Whatman Anodisc at 10 mM ionic strength (as KNO_3) measured using an Anton Paar surPASS electrokinetic analyzer.

Methods. To study the attachment of NPs to membranes, experiments were conducted at a constant ionic strength of 10 mM KNO_3 . The membranes were submerged in Ag NP suspensions for 3 h and pH was held constant using concentrated HNO_3 and KOH. A nitrogen blanket was used to minimize the introduction of atmospheric CO_2 . Amber glass containers were used to avoid degradation of the Ag NPs by light and the containers were placed on a shaker table throughout the experiment so that the suspensions remained mixed and to prevent Ag NPs from settling. The membranes were kept upright with a glass holder so that both sides were in contact with the Ag NP suspension at all times. The total suspension phase Ag concentration was measured using a Varian ICP-OES. To determine the amount of Ag deposited on the Anodisc, the filters were digested in concentrated HNO_3 to desorb the Ag.

Hypothesis 1 (that pH conditions can be selected according to DLVO theory, which promotes attachment) was tested by performing deposition experiments at both pH 5 and pH 7. These pH values were selected for several reasons. First, the pH values are below and above the point of zero charge for the Anodisc, but the sign of the charge for all three types of Ag NPs stayed the same. This allowed for testing scenarios where the particles and filters are of opposite sign (pH 5 for citrate and PVP Ag NPs, pH 7 for BPEI Ag NPs) and the same sign (pH 7 for citrate and PVP Ag NPs, pH 5 for BPEI Ag NPs). Second, the magnitude of the surface potential of the Anodisc stayed within the ± 25 mV constraint of using the linearized version of the double layer energy approximations. Finally, these pH values did not promote the dissolution of aluminum, so competitive adsorption is not a concern (Figure 4).

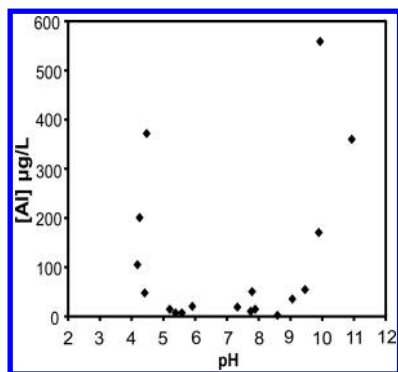


Figure 4. Anodisc's aluminum solubility measured using a Varian ICP-OES. Aluminum concentrations are very low for pH values of 5 to 9, the range of the experiments performed.

To test hypothesis 2 (systems with lower predicted DLVO energy barriers will experience greater Ag deposition), modeling was performed using Matlab on a number of scenarios that represent the experimental conditions (Table 2). Equations 5 and 6a (at constant

Table 2. Attachment Experimental Conditions

Ag NP	pH	Ag NP surface potential (mV)	anodisc surface potential (mV)	average particle radius (nm)	
				starting	ending
citrate	5	-23.4	14.5	6.5	9.2
	7	-29.1	-24.4		13.8
PVP	5	-9.8	14.5	7	10.8
	7	-9.3	-24.4		8.4
BPEI	5	33.8	14.5	7.8	14.5
	7	28.4	-24.4		20.9

potential) were used for comparison to experimental data. Experimentally obtained zeta potential measurements were converted to estimated surface potential values using the Gouy–Chapman model for characterizing the diffuse layer¹⁰

$$\psi = \frac{4k_B T}{ze} \tanh^{-1} \left(\tanh \left(\frac{ze\xi}{4k_B T} \right) \times e^{-\kappa d} \right) \quad (7)$$

where ξ symbolizes the zeta potential. A value of 5 Å was used for the distance, d , between the surface of the charged particle and the slipping plane.³³ Note that some researchers have used Oshima's model for soft particles to estimate the surface potential for particles with permeable layers.^{34,35} In this study, it was decided not to use this model because citrate and PVP are very thin layers and BPEI's branching violates the derivation assumptions. Still, it is important to recognize that the presence of the stabilizer will impact surface potential measurements and quantification. In the van der Waals attractive energy calculations, a value of 5.2×10^{-20} J was used for the Hamaker constant; this value was calculated using values for Ag, water, and Al_2O_3 provided in ref 16. Starting particle sizes were estimated from the particle size distributions in Figure 2a. Ending particle sizes were estimated using linear regression on the aggregation data presented in Figure 2b,c. The DLVO model was also tested at constant 5 and 10 nm radius values for all of the particles because as the particle radius changes, the DLVO energy barrier varies.

RESULTS

The magnitude of repulsive energy between the particles and membranes and, therefore, the height of the energy barrier depend on the approximation method (Figure 5). The constant charge assumption produces the largest repulsive energies, followed by (constant potential) LSA and constant potential. Although the energy barrier increases with increasing particle size, the order of repulsion/attraction among the different particle types and pH conditions does not change by the approximation method when run at radii of 5 and 10 nm and experimentally estimated starting and ending values (not shown). The scenario of all particles having a 10 nm radius is presented in this article, although it is recognized that differential particle sizes (both within and between particle types) can have a significant impact on BPEI Ag NPs. For example, for a 10-nm-radius citrate Ag NP, the energy barrier is larger (regardless of the approximation method) than that of a 10 nm BPEI or PVP Ag NP calculated by the same approximation method. However, if citrate Ag NPs are held constant at 10 nm, then their energy barrier is surpassed when BPEI Ag NPs are at 74 nm using the LSA, 26 nm using the constant charge approximation, or never using the constant potential approximation. (The difference in the surface potential of the Anodisc and particle is large enough that the approximation breaks down at short distances and always

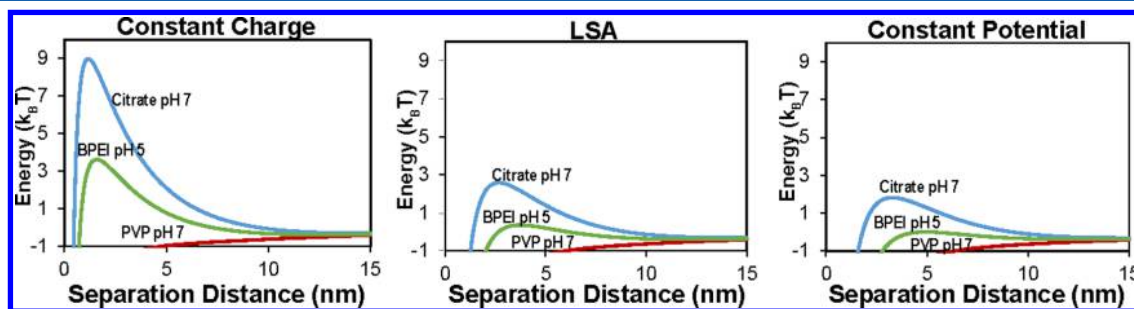


Figure 5. Energy barrier estimations using three different electrical double layer approximations. Scenarios represent Ag NP and Anodisc pH values where the particle and membrane have the same sign of the surface potential. All NPs were modeled using a 10 nm radius.

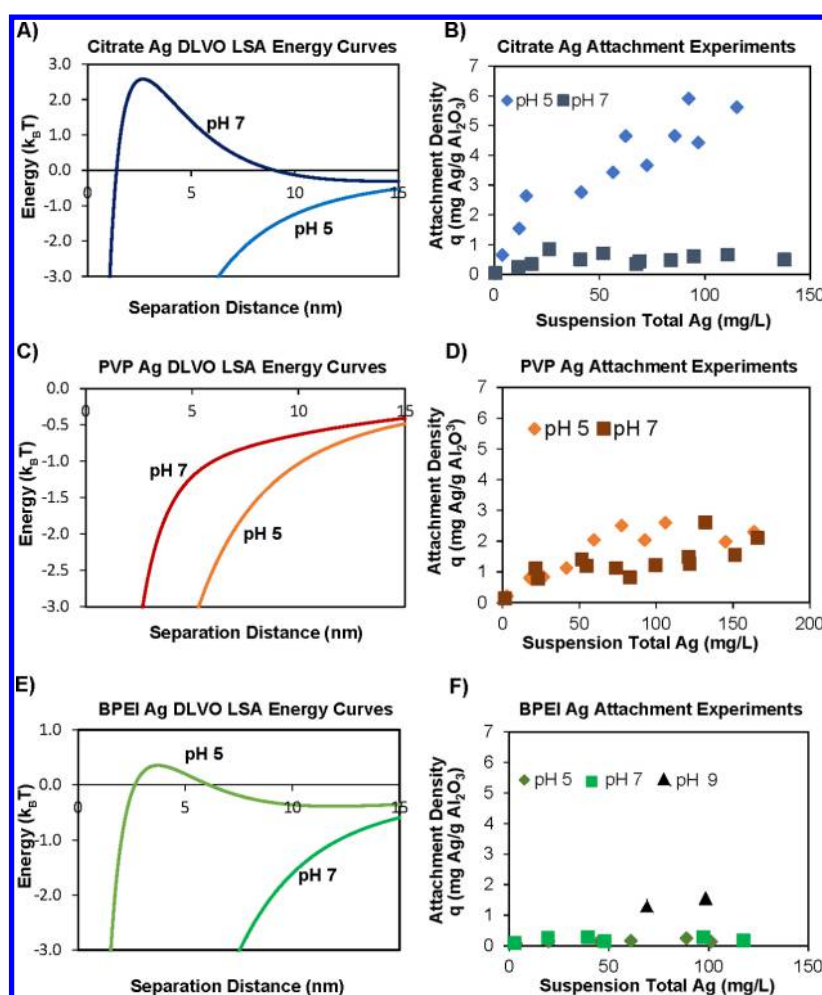


Figure 6. DLVO LSA modeling and attachment experimental results and pH 5 and 7. (A, B) Citrate Ag NPs, (C, D) PVP Ag NPs, and (E, F) BPEI Ag NPs. All NPs were modeled using a 10 nm radius.

produces attraction.) On the other hand, under all approximation methods, PVP Ag NPs' energy barrier never exceeds the citrate's energy barrier because as the particle size is increased, the van der Waals attractive energy and double layer repulsion both increase at comparable rates. Note that the κa value of the systems was 3.3 (where a = radius), which is generally considered to be $\gg 1$, meaning that the Derjaguin approximation is applicable.³⁶

Hypothesis 1 Results. The experimental results suggest that DLVO theory is effective at indicating pH conditions that promote attachment but that the degree of difference in deposition depends on the NP stabilizing agent (Figure 6). For electrostatically stabilized citrate Ag NPs, modeling (Figure 6A) predicts a large energy barrier for same sign surface conditions (pH 7) vs attraction under opposite sign surface conditions (pH 5). The experimental results (Figure 6B) demonstrate this phenomenon remarkably well.

On the other hand, modeling (Figure 6C) predicts attraction under all conditions for sterically stabilized PVP Ag NPs, with attraction starting at longer separation distances for pH 5 (opposite sign condition) than for pH 7 (same sign surface potential condition). Consistent with these results, the PVP Ag NP experimental results demonstrate a less pronounced pH dependence than do the citrate Ag NP experimental results (Figure 6D).

Some difference in the attachment at the two pH values occurs in the suspension with the total Ag concentration in the range of 50–125 mg/L, but at lower and higher concentrations, there is not a separation with pH. It is possible that the deposition at low PVP Ag NP concentrations is similar, regardless of pH, because the NPs are more spread out and do not experience strong lateral repulsive interactions among deposited and free particles. As the density of the coverage increases, the influence of the electrical double layer could play a more important role via lateral repulsive forces and thus produce a slight variation with pH. At concentrations higher than 125 mg/L Ag, an inversion of the surface potential of the deposited NP can occur which can lead to multilayer deposition or chemisorption. Multilayer deposition of PVP Ag NPs was observed using scanning electron microscopy (SEM), and an image is contained in the Supporting Information.

Despite an energy barrier for like sign conditions at pH 5 (Figure 6E), BPEI Ag NPs (electrosterically stabilized) demonstrate little difference in deposition at pH 5 vs pH 7 (Figure 6F). This insensitivity to pH indicates that the electrostatic interactions from the amine functional groups likely play a smaller role than the steric interactions between the BPEI molecule and the filter surface. If the pH of the solution is increased to pH 9, where the Anodisc surface potential is significantly lower (-40 mV, as shown in Figure 3), increased deposition can be induced (Figure 6F).

Hypothesis 2 Results. The DLVO modeling results predict that the order of least deposition to most deposition is citrate pH 7 < BPEI pH 5 < PVP pH 7 < PVP pH 5 < citrate pH 5 < BPEI pH 7 (Figure 7a). This order remains the same

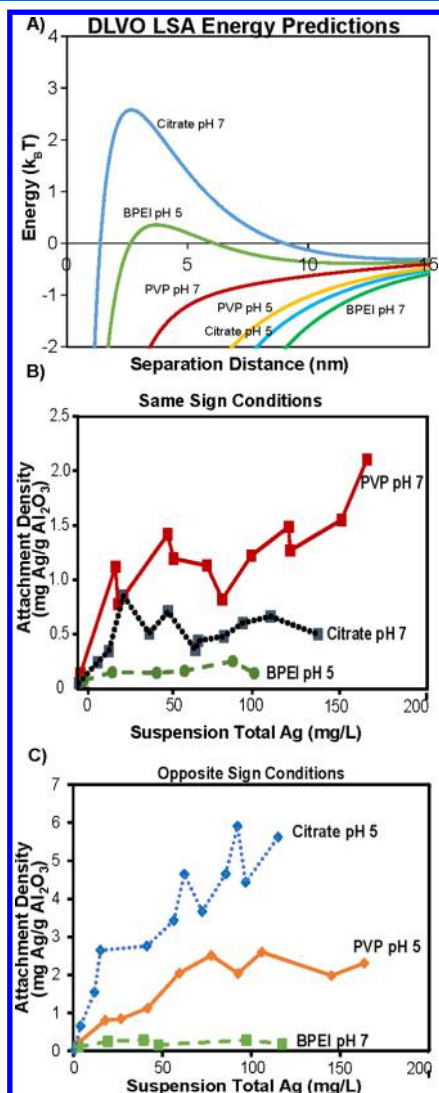


Figure 7. Theoretical (10 nm radius) and experimental Ag NP deposition order. (A) DLVO energy predictions calculated using the LSA method for the electrical double layer energy. (B) Experimental results for Ag NPs having the same sign surface potential as the membrane and (C) experimental deposition results for conditions where Ag NPs have the opposite sign to the surface potential of the membrane.

regardless of which electric double layer approximation method is used. Experimental results do not agree with this predicted order (Figure 7b,c). This disagreement suggests either that electrostatic interactions are not the dominant mechanism in NP attachment to the surface of ceramic water filters or that the origin of the surface charge or potential is different depending on the stabilizing agent. For same sign surface potential of the filter and NP, BPEI Ag NPs were predicted to have a lower energy barrier than citrate Ag NPs; however, they show less deposition. This disagreement could be due to several different physical phenomena. Steric interactions of the BPEI molecule or aggregation of BPEI Ag NPs over the course of the experiment could both cause less deposition of BPEI Ag NPs

than citrate. One way that the experimental deposition orders can be explained is by using different assumptions based on the type of stabilizing molecule. Interestingly, if the constant charge approximation method is selected to calculate the energy barrier for BPEI Ag NPs but LSA is used for the other NPs, then the order matches the experimental findings. Note that one might wonder if the flip in the energy barrier is induced by the fact that the constant charge assumption overestimates the exact solution for the energy barrier at close separation distances. However, the deviation between the exact and approximate solutions is not as large as the difference in solutions for the constant charge versus constant potential assumptions. It is imaginable that counterion charges could be trapped inside the long arms of the BPEI layer and thus be unable to escape at short times, lending credence to the constant charge assumption being more appropriate than LSA for estimating the energy barrier. On the other hand, PVP and citrate have been shown to form compact layers on NPs^{37,38} so LSA or a constant potential might be more appropriate. For conditions of the opposite sign surface potential of the filter and NP, the citrate Ag NP showed a more favorable deposition than was expected in comparison to the other types of NPs. Citrate was the only electrostatically stabilized particle, so it is quite reasonable to assume that other repulsive forces inhibit attachment for the particles that have steric stabilization.

Sterics. A widely employed theory to describe interactions between polymer layers is based on the Flory–Krigbaum theory. Lin and Weisner³⁹ derived the following energy expression for the osmotic contribution between a coated particle and an uncoated planar surface using this theory. (Their paper demonstrates that the elastic contribution is negligible.) Their model was validated using AFM results reported in the literature

$$\Delta G_{\text{self-mixing}} = k_B T \left(\frac{V_p^2}{v_s} \right) \left(\frac{1}{2} - \chi \right) \alpha_{s,\text{avg},\infty}^2 V_{1,s} \left(\frac{V_{1,s}}{V_3} - 1 \right) \quad (8)$$

where V_p is the volume of the polymer, v_s is the volume of a solvent molecule, χ is the Flory–Huggins solvency parameter, ϕ represents the segment density distribution, and $V_{1,s}$ and V_3 represent the volume for the polymer under different compression domains (this variable includes the separation distance). Matlab code was implemented to calculate the segment density distribution where the DLVO energy of interaction of citrate-Ag NPs was exceeded by BPEI Ag NPs. (Since the DLVO energy barriers occur at separation distances larger than the interpenetration distance for the thickness layers of citrate and PVP, steric interactions were calculated only for BPEI nanoparticles.) Assuming a uniform 10 nm layer of BPEI on the Ag NPs, the segment density distribution was varied. A conservative value of 0.45 for χ was used for BPEI (lower values would produce higher energy barriers/lower segment densities).

As more segments of BPEI are attached to the Ag core, the energy barrier (DLVO + sterics) increases until it reaches an energy value larger than the DLVO-only energy barrier for citrate Ag NPs at pH 7 (Figure 8). Using LSA electrical double layer estimations for both citrate and BPEI Ag NPs, 0.0045 nm⁻³ at pH 5 and 0.0114 nm⁻³ at pH 7 are required segment density distribution values that cause a less favorable deposition of BPEI Ag NPs than for citrate Ag NPs at pH 7 (the highest DLVO estimated energy barrier). These values are of the same order of magnitude regardless of the combination of boundary

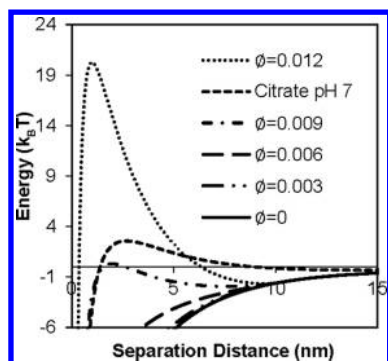


Figure 8. Effect of ϕ , segment density distribution (nm^{-3}), on the energies of interaction for BPEI Ag NPs vs citrate Ag NPs at pH 7. The LSA approximation is used for the electrical double layer and 10-nm-radius Ag NPs.

condition assumptions for the electrical double layer portion of the total interaction energy. BPEI Ag NPs at pH 7 require more segments than at pH 5 because pH 7 is where the membrane and particle have opposite sign surface potentials. Therefore, at pH 7, more electrostatic attraction must be overcome with steric interactions before unfavorable attachment conditions relative to citrate Ag NPs are observed. These values of the segment density distribution represent the number of polymer segments that must be attached uniformly to the volume surrounding the core of the NP, and they are not large values. This result indicates that a very small amount of BPEI is capable of providing substantial steric repulsion and thereby explains the experimental deposition order.

CONCLUSIONS

The type of stabilizing agents used in the production of Ag NPs affects the attachment of Ag NPs to ceramic water filters. Under similar conditions, citrate Ag NPs have the highest attachment affinity, followed by PVP Ag NPs and then BPEI Ag NPs. This result has implications of differential success rates for both the removal of unwanted particles from water and intentional adhesion to surfaces.

DLVO theory is effective at indicating pH conditions that promote increased deposition for citrate-stabilized Ag NPs. For particles that include steric stabilization, the results are not straightforward. A better understanding of the deposition of NPs on the ceramic membrane required systematic calculations of DLVO energy along with steric energy.

For electrostatically and electrosterically stabilized NPs, attachment to ceramic membranes is increased as the difference in opposite sign surface potential increases. This difference in surface potential leads to underestimations (constant potential) and overestimations (constant potential) of the linearized solutions to the Poisson–Boltzmann equation at short separation distances.

The influence of Ag NP size varies depending on the stabilizing agent and approximation method used to solve for the energy of interaction. The order of the energy barriers will switch for a 10 nm citrate Ag NP when BPEI Ag NPs are in the range of 26–74 nm. PVP and citrate Ag NPs do not switch energy barrier order as the size of the PVP Ag NPs changes.

For stabilizing molecules for which electrostatic effects are important, future research should be conducted on various stabilizing molecules to determine if constant charge or

constant potential is the more appropriate assumption for estimating double layer energy.

DLVO theory can make predictions only for a single particle and flat plate collectors. Depending on the stabilizing agent, NP solutions aggregate at different rates that are magnified by increasing concentration. Since larger particles lead to increased double layer repulsion, care should be taken to select the length of time to soak the filters in NP solutions such that the mixture of sizes does not inhibit deposition.

ASSOCIATED CONTENT

Supporting Information

The Supporting Information is available free of charge on the ACS Publications website at DOI: 10.1021/acs.langmuir.5b04675.

Ag NP synthesis procedures and characterization (TEM images and zeta potential curves); STEM stabilizer thickness measurements; Matlab code for the calculation of DLVO energy curves under different boundary condition assumptions; and determination of particle size that causes the energy barrier to exceed a set value (PDF)

AUTHOR INFORMATION

Corresponding Author

*E-mail: amikelonis@utexas.edu. Tel: +1-517-945-1531.

Author Contributions

The manuscript was written through the contributions of all authors. All authors have given approval to the final version of the manuscript.

Funding

We thank the American Water Works Association Abel Wolman Fellowship, the Nasser I. Al-Rashid Chair in Civil Engineering at the University of Texas at Austin, and the American Association of University Women Dissertation Fellowship for financial support over the course of this project.

Notes

The authors declare no competing financial interest.

ACKNOWLEDGMENTS

We used equipment located in the Texas Materials Institute for the STEM portion of the work, and we thank Dr. Shouliang Zhang for training and assistance. We also like thank Dr. Vinod Radhakrishnan at Anton Paar for analytical aid in obtaining the surPASS zeta potential curve for the Anodisc filter and Dr. Dwight Romanovicz for TEM training and assistance whenever needed.

ABBREVIATIONS

AFM	atomic force microscopy
BPEI	branched poly(ethylenimine)
DLVO	Derjaguin–Landau–Verwey–Overbeek
ICP-OES	inductively coupled plasma-optical emission spectra
LSA	linear superposition approximation
NPs	nanoparticles
NIST	National Institute of Standards and Technology
PVP	poly(vinylpyrrolidone)
PZC	point of zero charge
SEM	scanning electron microscope
STEM	scanning transmission electron microscope
Ag	silver

TGA	thermal gravimetric analysis
TEM	transmission electron microscopy
XPS	X-ray photoelectron spectroscopy

REFERENCES

- (1) Ng, L. Y.; Mohammad, A. W.; Leo, C. P.; Hilal, N. Polymeric Membranes Incorporated with Metal/metal Oxide Nanoparticles: A Comprehensive Review. *Desalination* **2013**, *308*, 15–33.
- (2) Wegmann, M.; Michen, B.; Luxbacher, T.; Fritsch, J.; Graule, T. Modification of Ceramic Microfilters with Colloidal Zirconia to Promote the Adsorption of Viruses from Water. *Water Res.* **2008**, *42*, 1726–1734.
- (3) Chen, Y.; Liu, X.; Liu, L.; Zhang, Y.; Wang, Z.; Zhang, Q. Functional Poly(vinylidene Fluoride) Membrane Anchored with Silver Nanoparticle with Antibacterial Activity. *Synth. Met.* **2013**, *174*, 1–5.
- (4) Byun, S.; Davies, S. H.; Alpatova, A. L.; Corneal, L. M.; Baumann, M. J.; Tarabara, V. V.; Masten, S. J. Mn Oxide Coated Catalytic Membranes for a Hybrid Ozonation-Membrane Filtration: Comparison of Ti, Fe and Mn Oxide Coated Membranes for Water Quality. *Water Res.* **2011**, *45*, 163–170.
- (5) Golas, P. L.; Louie, S.; Lowry, G. V.; Matyjaszewski, K.; Tilton, R. D. Comparative Study of Polymeric Stabilizers for Magnetite Nanoparticles Using ATRP. *Langmuir* **2010**, *26*, 16890–16900.
- (6) Goldstein, N.; Greenlee, L. F. Influence of Synthesis Parameters on Iron Nanoparticle Size and Zeta Potential. *J. Nanopart. Res.* **2012**, *14*, 760.
- (7) Bielefeldt, A. R.; Kowalski, K.; Summers, R. S. Bacterial Treatment Effectiveness of Point-of-Use Ceramic Water Filters. *Water Res.* **2009**, *43*, 3559–3565.
- (8) Kallman, E. N.; Oyanedel-Craver, V. A.; Smith, J. A. Ceramic Filters Impregnated with Silver Nanoparticles for Point-of-Use Water Treatment in Rural Guatemala. *J. Environ. Eng. (Reston, VA, U. S.)* **2011**, *137*, 407–415.
- (9) Oyanedel-Craver, V. A.; Smith, J. A. Sustainable Colloidal-Silver-Impregnated Ceramic Filter for Point-of-Use Water Treatment. *Environ. Sci. Technol.* **2008**, *42*, 927–933.
- (10) Benjamin, M. M.; Lawler, D. F. *Water Quality Engineering*; John Wiley & Sons: Hoboken, NJ, 2013; pp 315–318.
- (11) Adamczyk, Z.; Warszyński, P. Role of Electrostatic Interactions in Particle Adsorption. *Adv. Colloid Interface Sci.* **1996**, *63*, 41–149.
- (12) Cao, G. *Nanostructures & Nanomaterials: Synthesis, Properties & Applications*; Imperial College Press: London, 2004; pp 15–48.
- (13) Tolaymat, T. M.; El Badawy, A. M.; Genaidy, A.; Scheckel, K. G.; Luxton, T. P.; Suidan, M. An Evidence-Based Environmental Perspective of Manufactured Silver Nanoparticle in Syntheses and Applications: A Systematic Review and Critical Appraisal of Peer-Reviewed Scientific Papers. *Sci. Total Environ.* **2010**, *408*, 999–1006.
- (14) El Badawy, A. M.; Silva, R. G.; Morris, B.; Scheckel, K. G.; Suidan, M. T.; Tolaymat, T. M. Surface Charge-Dependent Toxicity of Silver Nanoparticles. *Environ. Sci. Technol.* **2011**, *45*, 283–287.
- (15) Silva, T.; Pokhrel, L. R.; Dubey, B.; Tolaymat, T. M.; Maier, K. J.; Liu, X. Particle Size, Surface Charge and Concentration Dependent Ecotoxicity of Three Organo-Coated Silver Nanoparticles: Comparison between General Linear Model-Predicted and Observed Toxicity. *Sci. Total Environ.* **2014**, *468–469*, 968–976.
- (16) Israelachvili, J. *Intermolecular and Surface Forces*, 2nd ed.; Academic Press: San Diego, 1992.
- (17) Anandarajah, A.; Chen, J. Single Correction Function for Computing Retarded van der Waals Attraction. *J. Colloid Interface Sci.* **1995**, *176*, 293–300.
- (18) Huynh, K. A.; Chen, K. L. Aggregation kinetics of citrate and polyvinylpyrrolidone coated silver nanoparticles in monovalent and divalent electrolyte solutions. *Environ. Sci. Technol.* **2011**, *45*, 5564–71.
- (19) El Badawy, A. M.; Scheckel, K. G.; Suidan, M.; Tolaymat, T. The impact of stabilization mechanism on the aggregation kinetics of silver nanoparticles. *Sci. Total Environ.* **2012**, *429*, 325–31.
- (20) Petosa, A. R.; Jaisi, D. P.; Quevedo, I. R.; Elimelech, M.; Tufenkji, N. Aggregation and deposition of engineered nanomaterials in aquatic environments: role of physicochemical interactions. *Environ. Sci. Technol.* **2010**, *44*, 6532–49.
- (21) Song, J. E.; Phenrat, T.; Marinakos, S.; Xiao, Y.; Liu, J.; Wiesner, M. R.; Lowry, G. V. Hydrophobic interactions increase attachment of gum Arabic- and PVP-coated Ag nanoparticles to hydrophobic surfaces. *Environ. Sci. Technol.* **2011**, *45*, 5988–95.
- (22) Gregory, J. Approximate expression for the interaction of diffuse electrical double layers at constant charge. *J. Chem. Soc., Faraday Trans. 2* **1973**, *69*, 1723–1728.
- (23) Gregory, J. Interaction of unequal double layers at constant charge. *J. Colloid Interface Sci.* **1975**, *51*, 44–51.
- (24) Tobiasson, J. E. Chemical effects on the deposition of non-Brownian particles. *Colloids Surf.* **1989**, *39*, 53–75.
- (25) Borkovec, M.; Behrens, S. H. Electrostatic double layer forces in the case of extreme charge regulation. *J. Phys. Chem. B* **2008**, *112*, 10795–9.
- (26) Carnie, S. L.; Chan, D. Y. Interaction free energy between plates with charge regulation: a linearized model. *J. Colloid Interface Sci.* **1993**, *161*, 260–264.
- (27) Elimelech, M.; Jia, X.; Gregory, J.; Williams, R. *Particle Deposition and Aggregation: Measurement, Modelling and Simulation*; Butterworth-Heinemann: 2013.
- (28) Usui, S. Interaction of electrical double layers at constant surface charge. *J. Colloid Interface Sci.* **1973**, *44*, 107–113.
- (29) Hogg, R.; Henly, T. W.; Furstenu, D. W. Mutual Coagulation of Colloidal Dispersions. *Trans. Faraday Soc.* **1966**, *62*, 1638–1651.
- (30) Verwey, E. J.; Overbeek, J. T. *Theory of the Stability of Lyophobic Colloids*; Elsevier: Amsterdam, 1948.
- (31) Furneaux, R. C.; Rigby, W. R.; Davidson, A. P. The formation of controlled-porosity membranes from anodically oxidized aluminum. *Nature* **1989**, *337*, 147–149.
- (32) Franks, G. V.; Gan, Y. Charging Behavior at the Alumina–Water Interface and Implications for Ceramic Processing. *J. Am. Ceram. Soc.* **2007**, *90*, 3373–3388.
- (33) van Oss, C. J. DLVO and Non-DLVO Interactions in Hectorite. *Clays Clay Miner.* **1990**, *38*, 151–159.
- (34) de Kerchove, A. J.; Elimelech, M. Relevance of Electrokinetic Theory for “Soft” Particles to Bacterial Cells: Implications for Bacterial Adhesion. *Langmuir* **2005**, *21* (21), 6462–6472.
- (35) Lin, S.; Cheng, Y.; Liu, J.; Wiesner, M. R. Polymeric coatings on silver nanoparticles hinder autoaggregation but enhance attachment to uncoated surfaces. *Langmuir* **2012**, *28*, 4178–86.
- (36) Glendinning, A.; Russel, W. The electrostatic repulsion between charged spheres from exact solutions to the linearized poisson-boltzmann equation. *J. Colloid Interface Sci.* **1983**, *93*, 95–104.
- (37) Park, J. *Interfacial Properties of Asymmetrically Functionalized Citrate-Stabilized Gold and Silver Nanoparticles Related to Molecular Adsorption*. Ph.D. Dissertation, UMI Number 3563410, The University of Utah, 2013.
- (38) Mdluli, P. S.; Sosibo, N. M.; Revaprasadu, N.; Karamanis, P.; Leszczynski, J. Surface Enhanced Raman Spectroscopy (SERS) and Density Functional Theory (DFT) Study for Understanding the Regioselective Adsorption of Pyrrolidinone on the Surface of Silver and Gold Colloids. *J. Mol. Struct.* **2009**, *935*, 32–38.
- (39) Lin, S.; Wiesner, M. R. Theoretical Investigation on the Steric Interaction in Colloidal Deposition. *Langmuir* **2012**, *28*, 15233–15245.